Patterning nanoscale flow vortices in nanochannels with patterned substrates

Siddharth Karakare, Abhimanyu Kar, Avinash Kumar, and Suman Chakraborty*
Department of Mechanical Engineering, IIT Kharagpur, Kharagpur 721302, India
(Received 26 August 2009; revised manuscript received 12 November 2009; published 29 January 2010)

We report the generation of complex toroidal nanoscale vortices in nanochannel flows, through the employment of patterned surface patches with contrasting wettability characteristics. Through extensive molecular-dynamics simulations, we further delineate that complicated interactions between the wettability gradient-driven vortex structures and surface roughness-influenced flow features may give rise to interesting patterns in the flow field. We also establish the orientation specificities of these nanoscale vortices, and demonstrate that the surface roughness effects may potentially act to alter the flow rotationalities realized out of modulated surface patterning effects to a considerable extent, which may have interesting consequences toward designing nanoscale mixing elements.

DOI: 10.1103/PhysRevE.81.016324 PACS number(s): 47.61.−k

The ability to generate featured structures over submicron [1,2] regimes has triggered a wide range of scientific investigations, encompassing several facets of interfacial fluid dynamics and molecular transport over nanometer length scales. Comprehensive studies have revealed that the affinity of fluids to nearby solid surfaces may be locally tuned through chemical treatment of the substrates, their topographical modulation, or by exploiting several nontrivial features of confinement-induced hydrodynamic interactions over reduced length scales, in a somewhat nontrivial fashion. However, while research studies have successfully demonstrated patterned vortex formation and mixing by utilizing these intriguing physico-chemical phenomena over microscopic scales, possibilities of realizing analogous effects over nanometer length scales have largely been unexplored. Such deficiencies in physical understanding have essentially stemmed from the fact that the classical paradigm of enhancing spatiotemporal mixing of fluid elements through chaotic advection appears to be virtually prohibitive in systems with characteristic length scales approaching only a few molecular dimensions, as attributable to their characteristic ultralow Reynolds number effects.

Several researchers have studied various important facets of hydrodynamics in nanometer scale channels through extensive molecular-dynamics (MD) simulations, elucidating interesting aspects of the underlying transport processes, including the effects of interface wettability on flow structures [3], fluid dynamics in surface-nanostructured channels [4], effects of wall lattice-fluid interactions on the density and velocity profiles [5], perturbations in fully developed pressure-driven flows [6], slip behavior on substrates with patterned wettability [7], and effects of surface roughness and interface wettability on nanoscale flows [8]. Issues of nanochannel transport of more complex fluids have also been elaborately addressed. For instance, Cieplak *et al.* [9] executed MD simulations of dense and rarefied fluids comprising small chain molecules in chemically patterned nanochannels, and predicted a novel switching from Poiseuille to plug flow along the channel. However, these studies were primarily directed toward unveiling the possible deviations of the velocity profiles from the classical parabolic shape, rather than emphasizing on multidimensionalities in the flow structure. Fan *et al.* [10] studied the effects of varying cross sections on the velocity vectors in nanochannel flows and concluded the possibilities of isolated vortical structure formation. However, possibilities of complex toroidal patterns in the flow field were not addressed in their work.

Can we realize patterned vortex structures with topographical complexities in pressure-driven nanochannel flows by overcoming these limits? Through extensive MD experiments, we demonstrate here that the above is indeed a possibility, by imprinting patterned patches of tunable wettabilities on nanochannel substrates with spatially varying topographical features, thereby rendering the flow system to be capable of shedding vortex structures which are reminiscent of typical recirculating rolls that may otherwise be observed only in confinements having lateral extents several orders larger in characteristic dimensions as compared to molecular scales. We also show that with a nontrivial interplay of the physical and topographical features of the confining boundaries, complex flow patterns may effectively be obtained with characteristic features varying over molecular dimensions, having favorable implications toward mixing enhancement through the combined advection-diffusion transport of vortex elements over spatiotemporal scales that are compatible with typical dimensions of nanoscale fluidic devices. We also demonstrate that surface roughness elements, which are inevitable artifacts of any fabrication process, may significantly perturb the vortex structures otherwise obtained as a consequence of patterning the surface wettability gradients.

Our MD simulations are essentially based on the employment of a generalized Lennard-Jones (LJ) potential for capturing the intermolecular interactions. Locally tunable wetting phenomena at the fluid-solid interface are simulated through a modified LJ potential, as $V(r_{ij})=16\varepsilon[(\frac{\sigma}{r_{ij}})^{12}-c(i,j)(\frac{\sigma}{r_{ij}})^{6}f(x_i,y_j)]$, where the parameter $c(i,j)$ may be utilized to mimic varying wettability characteristics. Lower and upper bounds in c conform to highly repulsive (nonwetting; $c=0$) and highly attracting (wetting; $c=1$) walls. In order to mimic the effects of atomically "corrugated" roughness char-

*suman@mech.iitkgp.ernet.in

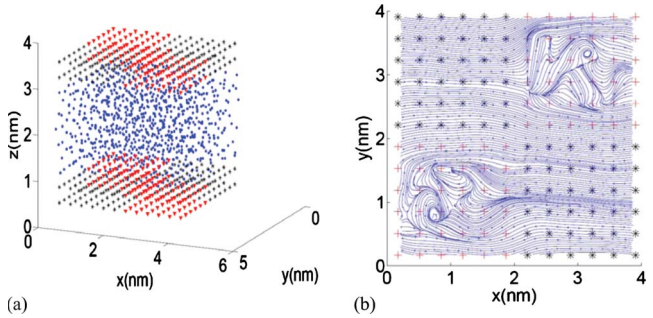

FIG. 1. (Color online) (a) Three-dimensional view of the system simulated. Triangles and asterisks indicate wall atoms, whereas circles represent fluid atoms. (b) Flow structures over a patterned arrangement of wall atoms. The "plus (+)" indicates hydrophilic wall atoms whereas the "asterisk (∗)" indicates hydrophobic wall atoms. The continuous lines indicate the streamlines of the flow.

acteristics of the surface, we modulate the attractive tail of the modified LJ potential with the following function:

$$f(x_i,y_j) = 1 + \frac{1}{3N}\sum_{K=1}^{3}\frac{1}{K}\left\{\cos\left(\frac{4\pi K}{b}x_i\right) + \cos\left[\frac{4\pi K}{b}\left(\frac{x_i}{2}+\frac{y_j\sqrt{3}}{2}\right)\right] + \cos\left[\frac{4\pi K}{b}\left(-\frac{x_i}{2}+\frac{y_j\sqrt{3}}{2}\right)\right]\right\}.$$

The parameter N implicates the amplitude of the surface asperities (smaller N implies rougher surfaces). In addition, the parameter K represents the wave number of the surface characteristics. Unlike the previous studies [8], choice of modified LJ potentials in this way not only allows a simultaneous control over the topographical and wettability characteristics of the confining boundaries through the pertinent interaction forces, but also implicates an explicit coupling between these two immensely consequential interfacial features. We consider the fluid atoms to be confined between two parallel walls, each consisting of two layers of atoms [see Fig. 1(a)] arranged in the [001] plane of a fcc lattice, with a lattice constant of 0.85σ [9]. The shortest distance between the two confining walls is taken as $H=6\sigma$. The fcc lattice in maintained by tethering the wall atoms to their lattice sites by a spring potential which is adjusted to keep rms deviation of the atoms from the lattice sites to zero. This essentially means keeping the wall atoms fixed and not allowing any deformation or oscillation about the lattice points [11,12]. Space between the two walls is filled with fluid atoms [marked by " *" in Fig. 1(a)]. A bulk fluid density of $\rho\sigma^3=1$ is considered for obtaining the results reported in this work. Periodic boundary conditions are employed in the x and y directions. Fluid properties considered resemble to those of liquid argon. Various parameters considered for the results reported here are as follows: $\varepsilon=0.9786$ kJ/mol; $\sigma=0.34$ nm; $b=12\sigma$; and $N=1,2$. The amplitude of roughness mimicked by $f(x,y)$ may be estimated as: $\Delta r=N^{1/6}\sigma[1-\frac{1}{\{\max(f)\}^{1/6}}]$, which is on the order of 0.1σ for $N=2$, for example. Such choices of parameters are sufficient to capture the essential physics of interactions between surface roughness and wettability conditions, without unnecessarily amplifying the computational complexity. Other choices of these parameters have also been extensively studied, but are not presented here for the sake of brevity. The physical scales pertinent to the simulation are interrelated as $\tau=\sqrt{\frac{m\sigma^2}{\varepsilon}}$, where σ is the molecular length scale, ε is the fluid-fluid interaction energy scale, and m is the molecular mass (taken as 39.948 a.m.u.) so that $\tau\sim 1$ ps. Each fluid atom is initially given a velocity that is randomly picked from the Maxwell-Boltzmann distribution, corresponding to a temperature of $1.6\varepsilon/k_B$ [9].

A variety of thermostat techniques has been introduced into the literature for adding and removing energy from the boundaries of the MD simulation domain in a realistic manner, so as to approximate the canonical ensemble. The Nosé-Hoover thermostat has been established as one such popular technique. The basic idea behind the Nosé-Hoover thermostat is to introduce a internal degree of freedom into the Hamiltonian of the system, which, in turn, modifies the equations of motion and introduces an additional governing equation for the thermostat variable. Importantly, calculations corresponding to this thermostat are executed in a reference frame in which center of mass of the system is at rest. This thermostat effectively introduces an "artificial" external frictional force, which is likely to alter the hydrodynamics. In addition, this thermostat does not conserve local momentum, primarily because of the fact that the effective thermostating forces are noncentral and nonpairwise additive. To circumvent the above problem, one may employ a modified Nosé-Hoover thermostat, as introduced by Stoyanov and Groot [11] by coupling two thermostats in parallel. The first one is a Galilean invariant version of the Nosé-Hoover thermostat that acts on pairs of atoms, rather than on a single atom. The second one is the Lowe-Anderson thermostat, which may be perceived as a pairwise analog of the Anderson thermostat. In the Lowe-Anderson thermostat, a pair of particles that are separated by less than a critical distance is selected to exchange momentum with a frequency of Γ. For each atom, the choice between the Nosé-Hoover thermostat and the Nosé-Hoover thermostat is made with a probability of $\Gamma\Delta t$, where Δt is the integration time step and Γ is the Lowe-Anderson exchange frequency. The resulting equations of motion are integrated using the velocity Verlet algorithm. In this way, a thermostating may be achieved that conserves both linear and angular momentum in the system. In the present case, however, results obtained by employing the Nosé-Hoover thermostat and those obtained by employing its modified version mentioned as above exhibit differences that are only marginal in nature. For implementation, the thermostat is applied during equilibration, while the system is then left free and allowed to equilibrate for 500 ps, with each time step being 0.001 ps long. Subsequently, an acceleration of $0.1\sigma/\tau^2$ is applied to all the fluid molecules along the positive x-direction. Our calculations have revealed that this is the threshold order of acceleration necessary to generate perceptible nanovortex formation in the wall-adjacent layers. The system is then allowed to equilibrate under this acceleration for another 500 ps. The LJ potential values are trun-

cated at 2.2σ. The equations of motion for individual molecules are integrated by using a velocity Verlet algorithm. The velocities and positions of the fluid atoms are sampled over a period of 80 ns. Averaging is done by employing cubical bins with size of each edge as σ.

We first discuss some representative results depicting relationships between the flow characteristics and surface wettability gradients. We consider a "checker box" arrangement of the hydrophilic and hydrophobic units on the channel walls [see Fig. 1(b) for a representative layout], using several types of repeating monoblocks as representative templates. Such units are carefully chosen to bring out the significance of wetting inhomogeneities amidst the existence of a structured patterning on disparate physical scales. Discontinuities in the solid-fluid intermolecular interactions essentially lead to jumps in the surface wettability conditions, resulting in fluid adsorption and layering on the attractive patches and depleted spaces near the repulsive patches. A competition between the designed wetting characteristics of the substrate and the imposed flow leads to fascinating flow patterns, with interesting morphological characteristics on a molecular scale [see Fig. 1(b) for a representative example]. Over the hydrophilic patches, the fluid tends to diffuse spontaneously, so as to minimize its free energy. However, the imposed flow tends to carry the fluid away from those "preferred" locations. If the channel walls merely contained single hydrophobic and hydrophilic patches, then that would have simply permitted the substrate-adhering fluid elements to be preferentially organized over the hydrophilic zone, while the external force would have trivially transported the outer flow over the wall-adjacent layers. The presence of alternate patches, each characterized by its own hydrophobic and hydrophilic subzones, interrupts this flow because locally varying wettability gradients over molecular scales. The fluid elements over local hydrophobic zones tend to adapt to their repulsive actions by diffusing into the bulk. However, because of spatial variations in the wettability conditions, the fluid can encroach partly into the incompatible subdomains. This leads to the inception of flow "arms" that sweep across the channel sections. These arms can join and pinch off, leading to interesting flow topologies even at the molecular scales. The flow structures typically exhibit asymmetric patterns, with their inceptions occurring at the junctions between adjacent surface elements having contrasting wettability characteristics. In the middle of the flow domain, the imposed external force tends to advect the flow elements with minimal explicit dependence on the surface patterning. However, because of molecular momentum transfer, the wall effects significantly diffuse into the bulk, aided by the narrow extent of the confinement. Thus, over a large extent within the domain, momentum diffusion dominates, resulting in upward, downward, and inclined movements of the flow arms and their intermingling, and eventually leading to necklacelike patterns. Overall, a complex interaction between advection in the bulk flow and momentum diffusion triggered by substrate wettability gradients as well as molecular momentum transfer between various layers effectively controls the evolution of the flow patterns in the system and are responsible for the observed intriguing flow characteristics. Importantly, these flow patterns not only depend on the relative extents of hydrophobic and hydrophilic patches on the walls, but also on their dominant orientations. This aspect is illustrated in Fig. 2, considering the examples of "horizontally" and "diagonally" laid out patches. In the later case, the hydrophobic diagonal forms a low resistance path for fluid flow, and vortex formation is observed in the hydrophilic regions on both sides of the diagonal, as a response to the driving force along x-direction. Interestingly, it is a differential gradient of fluid densities over the hydrophobic and hydrophilic patches that dictates the vortical structures in the flow and the interlayer mixing of the fluid elements. The density profiles corresponding to Figs. 2(a) and 2(b), as depicted in Figs. 3(a) and 3(b) aptly corroborate this viewpoint.

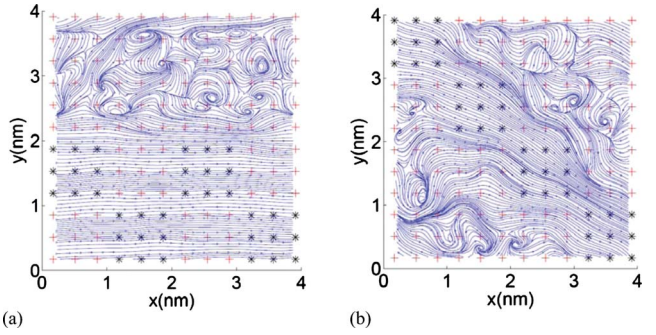

FIG. 2. (Color online) Flow pattern over the channel wall in "horizontally patched" and "diagonally patched" topologies. The "plus (+)" indicates hydrophilic wall atoms whereas the "asterisk (∗)" indicates hydrophobic wall atoms. The continuous lines indicate the streamlines of the flow.

How does the surface topology interact with the wettability gradients and influence the vortex structures? Typically, higher the degree of substrate-induced molecular ordering near an ideally flat (smooth) wall, less prominent is the degree of effective slip between the fluid and the solid [7], and greater is the momentum transfer between the fluid and the substrate. However, for rough surfaces with periodicities of comparable order as the periodicities in the surface wettability conditions, an interesting confluence may be observed, which can be attributed to an effective molecular-scale roughness corresponding to the heterogeneity in the liquid affinity along the substrate. The resultant flow features, considering combined effects of patterned surfaces with roughness effects, are elucidated in Fig. 4. The corresponding density profiles are shown in Fig. 5. Interestingly, it is revealed that for lower amplitude surface roughnesses (for example,

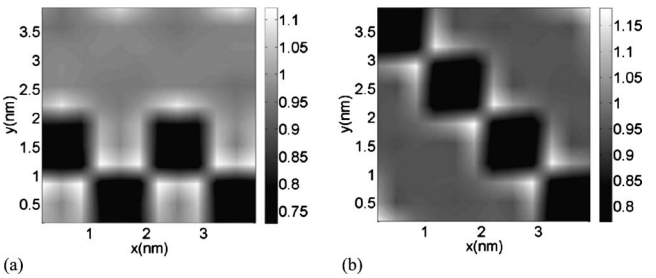

FIG. 3. Density field corresponding to the cases presented in Fig. 2

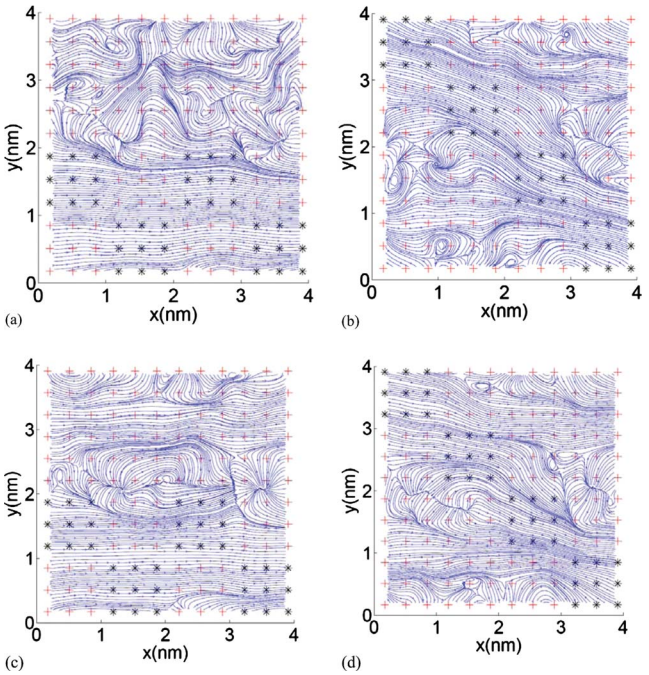

FIG. 4. (Color online) Flow patterns over rough channel surfaces with (a) and (c) "horizontally patched" and (b) and (d) "diagonally patched" configurations. Cases (a) and (b) correspond to $N=2$, whereas cases (c) and (d) correspond to $N=1$. The "plus (+)" indicates hydrophilic wall atoms whereas the "asterisk (∗)" indicates hydrophobic wall atoms. The continuous lines indicate the streamlines of the flow.

$N=2$), the vortex formation is essentially surface patterning dominated [see Figs. 4(a) and 4(b)], whereas for higher amplitude cases (for example, $N=1$), the same is essentially surface roughness dominated [see Figs. 4(c) and 4(d)]. In the later cases, the flow rotationalities are significantly affected by high-amplitude roughness elements.

In order to quantitatively compare the rotational strengths

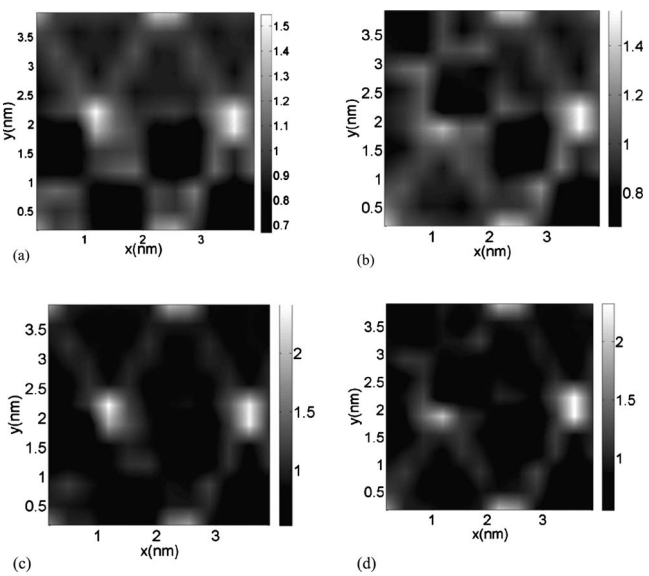

FIG. 5. Density field corresponding to the cases presented in Fig. 4

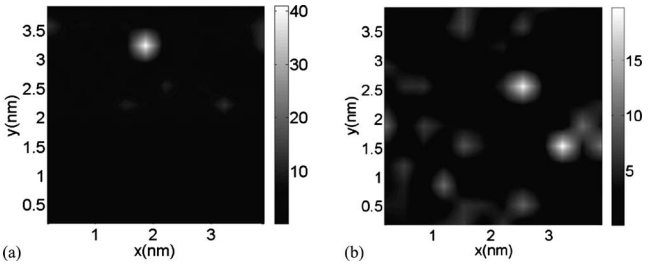

FIG. 6. Dimensionless vorticity (C_z) fields corresponding to the cases presented in Fig. 2

in the flow structures for rough and smooth surfaces, we obtain the field distribution of a rotationality parameter $C_z=\sigma|\frac{\vec{\nabla}\times\vec{V}}{\vec{V}}|_z$, which is essentially a dimensionless vorticity component along the z-direction. Contours of the dimensionless vorticities, corresponding to the cases reported in Figs. 2 and 4, are delineated in Figs. 6 and 7. Local cross gradients of densities because of patterned wettabilities essentially give rise to local rotationalities in the flow structure, as influenced by wall roughness elements. Upscaled interpretation of such typical flow structures may also be offered qualitatively from a quasicontinuum perspective, as described in our subsequent discussions. The root mean square of the surface roughness parameter C_z, as denoted by C_{rms}, is indicated in Table I for two representative cases. Interestingly, the surface roughness effects have two contrasting influences. On one hand, these act to reduce the strengths of flow rotationalities by destroying the localized toroidal vortices, and on the other hand these tend to enhance the overall rotational strengths by introducing local sources or sinks around a central band in the flow structure. The net effect turns out to be an enhanced C_{rms} with the interplay of surface roughness elements, as evident from Table I.

In order to assess the implications of the extent of domain confinement and the numbers of fluid atoms on the conver-

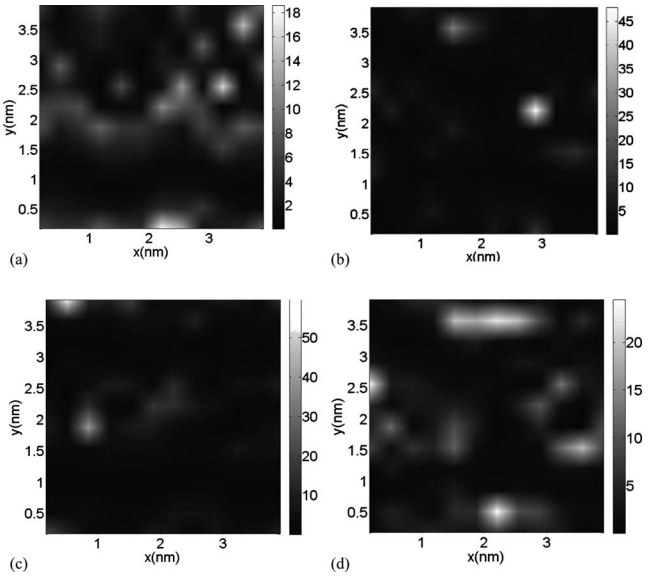

FIG. 7. Dimensionless vorticity (C_z) fields corresponding to the cases presented in Fig. 3

TABLE I. Dimensionless rms vorticity comparisons for smooth and rough walls.

Pattern	C_{rms} without roughness	C_{rms} with $N=1$
Horizontally patched	4.98	8.21
Vertically patched	3.49	7.18
Diagonally patched	4.23	6.05

gence of the MD solutions, we have varied the domain size and number of fluid atoms for the chosen bulk fluid density, and have repeated the simulations under those varied conditions. In particular, we have studied fluid domains with vertical extents of $H=6\sigma,8\sigma,10\sigma$, by employing 864, 1152, and 1440 numbers of fluid atoms, respectively (with a reference dimension of $12\sigma\times12\sigma$ in the x-y plane). We have observed that the dimensionless vorticity number (C_{rms}) remains virtually unchanged with these alterations, with identical vortical structures obtained corresponding to any given combination of surface wettability and roughness characteristics. Since plots for such different case studies are virtually repetitive with those presented in the paper, we have omitted their reproduction for the sake of brevity.

How can we explain the qualitative physics of the nanoscale vortex formation from an upscaled quasicontinuum perspective? It is qualitatively conjectured that over the system length scales, surface roughness-wettability coupling may give rise to an effective stick-slip motion. Nonwetting surface units are not thermodynamically favored to form attractive bonds with the fluid molecules. Hence, these give rise to excluded volume regions encompassing the locations characterized with sharply diminishing number density of the fluid. Close to isolated nonwetting units, the fluid molecules can structurally change and reorganize without sacrificing their attractive interactions. However, with repeated nonwetting units, persistence of a sustained network of attractive bonding is virtually impossible. Such interfacial perturbations may destabilize the liquid further away from the solid walls, leading to significant pressure perturbations, and hence gradients in transverse as well as axial flow velocity components. In confined fluids, long-ranged interactions may also trigger separation-induced instabilities, which may physically originate from an enhancement in the local molecular field due to an effective replacement of the fluid by solid walls. The localized but repeating patches of nonwetting surface units tend to catalyze the variations in these effects to a significant extent. The net effect at the solid boundary may be conceptualized in a continuum perspective by introducing locally variable slip-stick lengths, consistent with the coupling between surface wettability and topographical characteristics. Over the surface roughness length scales, a flow may be locally induced, which can dissipate mechanical energy and therefore can resist motion. Mathematically, the problem can be transformed into an equivalent stick-slip boundary condition on an idealized flat wall, with an appropriate accounting of the pertinent geometrical and statistical information on the topographical features of the corrugated surface [13]. The effective slip length, l_s, resulting from these features, may be considered to obey the

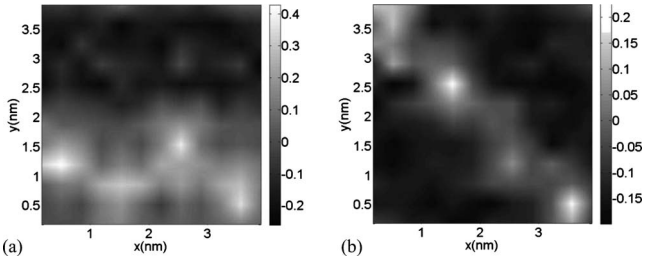

FIG. 8. Slip length map corresponding to the cases presented in Fig. 2

following generalized boundary condition on a continuum scale [14]: $l_s(\nabla_k V_i+\nabla_i V_k)t_i n_k=V_i t_i$, where **n** is a unit vector normal to the interface and pointing toward the liquid and **t** is a unit vector in its tangential direction. The local variations in l_s over the surface patterning length scales becomes nontrivial, considering the complex interactions between the topographical and wettability features of the confining boundaries. At locations where the reduced surface wettability dominates significantly over the "topographical drag," the values of l_s are higher, whereas at other locations those may be lower. To simplify the explanation and yet isolate the essential physics, one may consider a reduced system in which the local slip length varies along x, as $l_s=l_s^{(0)}[1+a\cos(kx)]$, which in turn gives rise to a continuity-satisfying transverse velocity component [15]

$$V_z(z) = kV_x\left(\frac{al_s^0}{H}\right) \times\cos(kx)\frac{(H-z)\sinh k(H+z)-(H-z)\sinh k(H-z)}{\sinh 2kH+2kl_s^0\cosh 2kH-4k(H-z)},$$

which is accurate up to the first order in a. Since l_s varies on a locally patterned scale, existence of such spatially varying axial and transverse velocity components with designed pe-

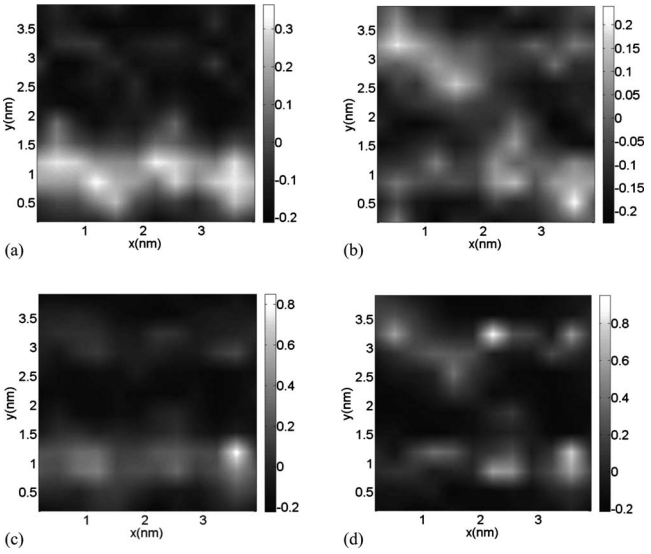

FIG. 9. Slip length map corresponding to the cases presented in Fig. 4

riodicities give rise to wall-adjacent nanoscale vortex elements in the flow structure. The vorticity perturbations on account of variations in surface wettability get effectively transmitted into the outer layers due to intricate intermolecular interactions, thereby giving rise to fascinating flow structures as delineated earlier. While being qualitatively physical, it may however be noted that the above oversimplified qualitative argument may get substantially more involved corresponding to the real three-dimensional nature in the patterned "slip" behavior considered in the present study, giving rise to both x and y dependences in l_s. Nevertheless, the essential physics of obtaining patterned nanoscale vortices, even in such complicated cases (as evident from the MD simulations presented here), remains conceptually analogous to what is portrayed in this elusively simple explanation from an equivalent continuum perspective. This facet may also be illustrated through the slip length maps as depicted in Figs. 8 and 9, corresponding to the cases presented in Figs. 2 and 4. Following the Navier boundary condition, these slip lengths are calculated by extrapolating the velocity profiles from the respective near-wall positions in the fluid to a hypothetical location where the velocity would vanish. In terms of the slip velocity (u_s) at the wall location, the slip length (l_s) is thus estimated as

$$l_s = \frac{u_s}{\left(\frac{dV_x}{dz}\right)_{wall}}.$$

Clearly, strong gradients of slip lengths occur across the boundaries of the regions demarcating dominant and abundant existence of nanoscale vortices, as evidenced through Figs. 8 and 9.

In summary, we have demonstrated through MD simulations that half-toning-like patched elements on nanochannel substrates with varying wettabilities may give rise to interesting rotationalities in the flow structures, very much akin to the flow vortices that may otherwise be obtained only at substantially elevated Reynolds numbers. In addition, we have illustrated the interactions between these structures and surface roughness elements, and have elucidated that the later ones may effectively act in dramatically modulating the rotationalities in the resultant flow structure. We have also introduced a quantification of the vorticity field in the nanoscale domain as a function of relative orientations of the surface patches, which may offer design insights to the science and technology of nanoscale mixing.

[1] G. M. Whitesides and A. D. Stroock, Phys. Today **54** (6), 42 (2001).
[2] S. D. Gillmor, A. J. Thiel, T. C. Strother, L. M. Smith, and M. G. Lagally, Langmuir **16**, 7223 (2000); T. P. Russell, Science **297**, 964 (2002).
[3] G. Nagayama and P. Cheng, Int. J. Heat Mass Transfer **47**, 501 (2004).
[4] B.-Y. Cao, M. Chen, and Z.-Y. Guo, Phys. Rev. E **74**, 066311 (2006).
[5] C. Y. Soong, T. H. Yen, and P. Y. Tzeng, Phys. Rev. E **76**, 036303 (2007).
[6] A. S. Ziarani and A. A. Mohamad, Microfluid Nanofluid **2**, 12 (2005).
[7] N. V. Priezjev, A. A. Darhuber, and S. M. Troian, Phys. Rev. E **71**, 041608 (2005).
[8] S. C. Yang, Microfluid Nanofluid **2**, 501 (2006).
[9] M. Cieplak, J. Koplik, and J. R. Banavar, Phys. Rev. Lett. **96**, 114502 (2006).
[10] X.-J. Fan, N. Phan-Thien, N. T. Yong, and X. Diao, Phys. Fluids **14**, 1146 (2002).
[11] P. A. Thompson and M. O. Robbins, Phys. Rev. A **41**, 6830 (1990).
[12] M. Cieplak, J. Koplik, and J. R. Banavar, Phys. Rev. Lett. **86**, 803 (2001).
[13] S. D. Stoyanov and R. D. Groot, J. Chem. Phys. **122**, 114112 (2005).
[14] D. Einzel, P. Panzer, and M. Liu, Phys. Rev. Lett. **64**, 2269 (1990).
[15] S. C. Hendy, M. Jasperse, and J. Burnell, Phys. Rev. E **72**, 016303 (2005).